Soft Matter

RSC Publishing

PAPER

View Article Online
View Journal | View Issue

Membrane insertion of sliding anchored polymers†

Cite this: *Soft Matter*, 2013, **9**, 1700

Martin Bauer,[ab] Max Bernhardt,‡[a] Thierry Charitat,[b] Patrick Kékicheff,[b] Christophe Fajolles,[a] Giovanna Fragneto,[c] Carlos M. Marques[b] and Jean Daillant§*[a]

Received 24th August 2012
Accepted 23rd November 2012

DOI: 10.1039/c2sm26972d

www.rsc.org/softmatter

We have studied the insertion into lipid bilayers of Sliding Anchored Polymers (SAPs), a new class of macromolecules based on topological complexes between end-capped polyethylene glycol (PEG) polymers and mono-cholesteryl cyclodextrins (CD). By using Infra Red Reflection Absorption Spectroscopy (IRRAS) we demonstrate that these new sliding polymer complexes anchor well in phospholipid model membranes self-assembled from DPPC. The in-plane organization is characterized by Brewster Angle Microscopy (BAM) at the air–water interface and by Atomic Force Microscopy (AFM) for lipid monolayers and for lipid bilayers deposited on mica. Demixing between SAPs and the phospholipids is observed even at low surface pressures. Using neutron reflectivity, we show that for sufficiently high polymer densities the SAPs inserted into lipid monolayers and lipid bilayers form polymer brushes, consistent with theoretical predictions for polymers with a sliding anchor.

1 Introduction

End-grafted chains have acquired in the field of macromolecular science the stature of a paradigmatic polymer interfacial geometry.[1] Grafted as a dense brush layer,[2] the chains interact strongly and stretch outwards from the grafting plane, providing a robust steric repulsion for applications in many colloidal and biomimetic system: stabilization of industrial formulations such as paints,[3] mineral recovery, lubrication and wetting control,[4] stealth protection from the immune systems in liposomal formulations for drug delivery,[5] only to name a few. Sparsely end-grafted, in the so-called mushroom regime, the end-grafted chain allows for probing many of the equilibrium and out-of-equilibrium properties of single polymer chains, such as surface induced depletion[6] and the resulting localized polymer-induced pressure,[7] stretching and recoiling under shear,[8] collapse and stretching following changes in solvent quality or electrostatic interactions,[9] *etc.* In the biological realm, the end-grafted chain has also been studied as a mimetic system for the spacers that provide for control of the range and strength of interactions in bio-recognition events promoted by ligand–receptor pairs.[10]

The applied and fundamental importance of the end-grafted polymer layers has driven many efforts to control the properties of the interfacial structure by molecular design of the anchored polymers including control of chain length and architecture,[11] monomer-sequence design[12] and attachment of end-functional groups, and by tuning the density and attachment mode of the chains. For instance, large densities have been sought by grafting from melts or by *in situ* growing of the polymer layers,[13,14] while lateral mobility has been achieved by anchoring hydrophobically modified polymer chains in micellar, worm-like and bilayer self-assemblies.[15]

Recently, it has been theoretically proposed that polyrotaxanes, the inclusion complexes formed between a polymer and a ring-like molecule, could lead to a new class of grafted polymer layers whereby the attachment point between the chain and the substrate would allow the chains to slide freely, while being prevented from escaping by a capping group at each chain-end.[16] This form of chain attachment to a surface leads to a new class of polymer interfacial structure, that we name Sliding Anchored Polymers, or SAPs, with many new interesting potential features from the point of view of both equilibrium and dynamic layer properties.

The SAPs presented in this paper are polyrotaxanes which have been built by a combination of polyethylene glycol (PEG) polymers and α-cyclodextrins, mono-functionalized with a cholesteryl group, as depicted in Fig. 1. Escape of the polymer from the sliding anchoring ring is prevented by 2,5-dimethoxyphenyl-1-ethyl (DMPE) end-caps. DMPE was chosen to be large enough to prevent dethreading of the cyclodextrin rings while keeping hydrophobic interactions as small as possible. Polyethylene glycol (PEG) polymers and α-cyclodextrins are well

[a]*CEA, IRAMIS, SIS2M, LIONS, UMR 3299 CEA/CNRS, CEA-Saclay bât. 125, F-91191 Gif-sur-Yvette Cedex, France. E-mail: Jean.Daillant@synchrotron-soleil.fr; Fax: +33 1 6908 6640; Tel: +33 1 6908 6481*

[b]*Institut Charles Sadron, University of Strasbourg, CNRS, 23 Rue du Loess, BP 84047, 67034 Strasbourg Cedex 2, France*

[c]*Institut Laue-Langevin, 6 rue Jules Horowitz, BP 156, 38042 Grenoble Cedex, France*

† Electronic supplementary information (ESI) available. See DOI: 10.1039/c2sm26972d

‡ Present address: Max Planck Institute for Polymer Research Ackermannweg 10 55128 Mainz.

§ Present address: Synchrotron SOLEIL, L'Orme des Merisiers, Saint-Aubin, BP 48, F-91192 Gif-sur-Yvette Cedex, France.

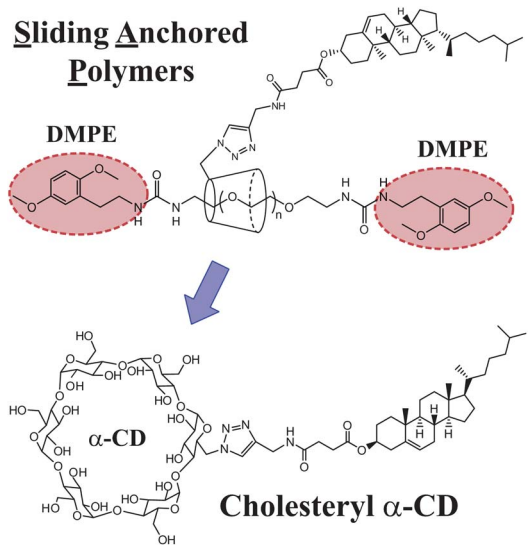

Fig. 1 Structure of a SAP, which is a polyrotaxane using a PEG polymer backbone, with a threaded cholesteryl α-CD and end-capped with 2,5-dimethoxyphenyl-1-ethyl (DMPE) stoppers.

known to easily give channel-like inclusion complexes with high to medium polymer coverage.[17] Statistical grafting capabilities of threaded α-cyclodextrins have been exploited for recognition[18] and also for sliding crosslinking by linking different CDs, bringing typical softness to the material.[19,20] In this paper, on the contrary, the ideal structures for SAPs are polyrotaxanes with only one or two sliding rings per chain[16] (see Fig. 1). As a supplementary constraint, each ring (CD) had to bear specifically one modification in order to graft one desired lipophilic anchor. Cholesterol is known for its ability to insert CDs[21–23] as well as PEG[24,25] in membranes. The linker plays a key role for the effective insertion of CDs[21] and also for PEG.[25] Cholesterol hemisuccinate was then chosen as an efficient[23] commercially available building block and as a cleavable ester linkage.[26]

By using a range of surface probing techniques, we study the insertion properties and the structure of this new family of interfacial polymer structures in lipid monolayers and in lipid bilayers, with a special emphasis on the SAP insertion behavior at a molecular scale.

2 Experimental section

2.1 Synthesis of the SAPs

The synthesis of the SAPs is described here briefly. More details can be found in the ESI.† DPPC (1,2-dipalmitoyl-*sn-glycero*-3-phosphocholine), chloroform (stabilized with ethanol) and methanol were purchased from Sigma-Aldrich. For the neutron reflectivity experiments, chain-perdeuterated dipalmitoylphosphatidylcholine (DPPC-d_{62}) was bought from Avanti Polar Lipids and deuterium oxide (99.85%D, Euriso-top) was provided by ILL. Ultra pure water (18.2 MΩ cm) is obtained from a Millipore purification system.

Briefly, a mixture of 6-monoazido-α-cyclodextrin (ACDN3) (Biocydex, France) and bis-amino-terminated polyethylene glycol (PEG-BA) (Aldrich) is prepared by a modification of the Fleury *et al.* method to produce a controlled inclusion compound in water as a soluble pseudopolyrotaxane.[27] The polyrotaxane is then obtained in the same pot as bis-1,3-dimethoxy-2-phenyl-ethyl (DMPE) urea. DMPE is large enough to prevent ACDN3[27] dethreading. The average number of CDs per chain is determined by comparison of the [^{1}H] NMR isolated peaks integration of aromatic urea and cyclodextrin. The monoazido moiety of the cyclodextrin is then clicked with the appropriate alkyne under Finn's general conditions,[28] adapted with a carefully chosen solvent. Full details for the polyrotaxanes preparation will be described separately.

The reference compound cholesteryl-α-cyclodextrin is prepared in a similar manner by clicking ACDN3 and cholesteryl-succinic acid propargylamide. The cholesteryl-α-cyclodextrin was found to be insoluble in water and chloroform, but soluble in aprotic dipolar solvents as DMSO (NMR) and in a chloroform–methanol 4 : 1 mixture as reported earlier for cholesteryl-cyclodextrins.[21] Owing to the PEG moiety, SAPs gain solubility in water as well as in organic solvents. The SAPs prepared and used in this study (Table 1) comprised a very small average number of CDs per chain. That implies that the statistical mixture consists mainly in polymer chains bearing respectively 0, 1 or 2 CDs per chain with ratios specific to each SAP and specifically one cholesterol pendant attached to each CD. Aggregation processes in water, due to the amphiphilic nature of SAPs, should thus be complex and measurements such as critical aggregation concentrations were not carried out as this study is focused instead on their insertion properties into phospholipid membranes.

2.2 Langmuir isotherms

The surface pressure–area isotherms are measured with a temperature controlled Langmuir balance used under a Brewster Angle Microscope (702BAM Film Balance for Brewster Angle Microscopy, Micro-Processor Interface IU4, NIMA Technology). Its maximum surface area is 700 cm^2, the minimum surface area 80 cm^2 and it is filled with approximately 500 ml of ultra pure water (18.2 MΩ cm). A solution of the SAPs in chloroform–methanol 4 : 1 is spread on the water surface. The surface pressure Π is measured by the Wilhelmy plate method. After 15 min of equilibration of the monolayer, the isotherms are recorded with a compression speed of 10 cm^2 min^{-1} at a temperature of 20 °C, unless otherwise stated. The compression ratio of our Langmuir trough (9 : 1) is not sufficient to record the isotherms for samples with SAP molar ratios >10% in one run for the whole surface area range. Depending on the

Table 1 Composition of SAPs (Fig. 1) used in experiments and their abbreviation in the text

Compound	N_{CD}	M (PEG) [kg mol^{-1}]
SAP-3k	1.2	3
SAP-6k	1.5	6
SAP-10k	1.5	10
SAP-20k	1.4	20
SAP [2.6]-20k	2.6	20

composition and Molecular Weight (MW) of the SAP, two or three isotherms have been measured for different surface concentrations and put together to obtain the full isotherm. Especially for high SAP ratios and high MW, the isotherms for lower surface concentrations have to be shifted with respect to the surface area in order to be connected. We have decided to displace all data with respect to the isotherm recorded with the highest surface concentration, which gives results consistent with the literature.[29,30] An example can be found in the ESI.† The SAPs used to prepare Langmuir monolayers are listed in Table 1.

2.3 Infra-red reflection-absorption spectroscopy

Infrared reflection absorption spectroscopy (IRRAS) is performed with a Bruker Vertex 70 IR apparatus co-aligned with a Langmuir trough. The surface has been irradiated with *p*-polarised light from a NIR/MIR source in the range of 8000–200 cm^{-1} at an angle of incidence of 40°. The light is detected with a liquid nitrogen-cooled MCT detector and the polarisation of the light is controlled by a HINDS PEM-100 polariser. The whole setup is sealed with a Plexiglas hood and purged with nitrogen. In order to avoid interference of water vapor, spreading solvent and CO_2, the trough shuttle technique is applied. The spectra have been analysed with the OPUS 6.0 software (Bruker). The sample trough and reference trough are filled with a millipore water subphase. After spreading of the sample the system has been allowed to equilibrate for 30 min prior to measurement. The film has been compressed with movable barriers and IR spectra have been collected at the desired surface pressures.

2.4 Neutron reflectivity

Specular reflectivity, $R(q)$, is defined as the ratio between the specularly reflected and incoming intensities of a neutron beam, which is measured as a function of the wave vector transfer, $q = 4\pi/\lambda \sin \Theta$, perpendicular to the reflecting surface, where Θ is the angle and λ the wavelength of the incoming beam. $R(q)$ is related to the scattering length density profile across the interface by the square modulus of its Fourier transform. Therefore the phase is lost and the data need to be fitted with an appropriate model to obtain the density profile. In this manner it is possible to determine film profiles within Å precision.[31,32] The data were fitted with the ProFit package 6.2 (QuantumSoft), where the specular reflectivity is calculated by the Abeles matrix method for stratified interfaces.[33] For samples where different contrasts were measured, the fits were conducted in a coupled manner, where only the SLDs of the subphase are allowed to vary (corresponding figures can be found in the ESI†). The error bars were determined by varying each parameter of the model and evaluating the χ^2 parameter, as well as by visually checking the quality of the fit.

Monolayers. Mixed monolayers containing 3, 10, 30 and 100 mol% SAP were prepared, using deuterated DPPC-d_{62}. The CD/phospholipid samples, dissolved in chloroform–methanol 4 : 1, were spread in a Langmuir trough (Nima), which is perfectly aligned with the neutron beam and filled with a water subphase. The trough was sealed with a Plexiglas cover and the solvent was allowed to evaporate for 15 min prior to film compression to the desired surface pressure. The reflectivity curves were recorded for each surface pressure at three different subphase contrasts, such as D_2O (SLD = 6.34×10^{-6} $Å^{-2}$), 4 matched water (4MW SLD = 4.0×10^{-6} $Å^{-2}$) and silicon matched water (SMW, SLD = 2.07×10^{-6} $Å^{-2}$) to remove the ambiguities of the fit.

The neutron reflectivity experiments at the air–liquid interface were carried out at the time of flight reflectometer FIGARO (Fluid Interfaces Grazing Angles Reflectometer) at the ILL, Grenoble.[34,35] The incoming beam comprises wavelengths between 2 Å and 30 Å. For our samples a *q*-range 0.005–0.30 $Å^{-1}$ could be achieved by joining two measurements together, with reflection angles $\Theta_1 = 0.62°$ and $\Theta_2 = 3.82°$ and a resolution of 5.6%. The samples are measured in a Langmuir trough (Nima) with a maximum and minimum area of 930 cm^2 and 254 cm^2 respectively. The reflectivity was normalised by direct beams in a transmission geometry through the windows of the Langmuir trough lid, and corrected for incoherent background scattering. For details on the variable resolution options of the two instruments please see ref. 34 and 35.

Bilayers. The bilayers were prepared on $5 \times 5 \times 1$ cm^3, homogeneously n-doped silicon single crystals, oriented [111] on the side where the film is deposited and atomically smooth with a roughness <5 Å, as determined by the manufacturer (SILTRONIX, Archamps, France). Prior to each deposition, the silicon block was cleaned with chloroform, ethanol and water, and then treated with UV/ozone for 30 min to reach a hydrophilicity as high as possible. For all bilayers, deuterated DPPC-d_{62} was used.

The double layer deposition was carried out on a (1300×300 cm^2) NIMA trough. The first layer was deposited by the classical Langmuir–Blodgett technique, whereas the second layer was deposited by the Langmuir–Schaefer method (horizontal sample) at 40 mN m^{-1} and the temperature was kept constant at 20 °C. The samples were then inserted into a Teflon sample cell, which was put into an aluminum box to be mounted on the neutron reflectometer and thermostatted using a water circulation bath. The cell was connected to a solvent circuit by means of a peristaltic pump in order to be able to change the subphase for different contrast. More detailed information about the substrate and sample preparation has been given elsewhere.[31]

The bilayers have been prepared with a first pure phospholipid monolayer close to the silicon substrate and a second mixed layer exposed to the water subphase (the detailed sample composition is given in Table 2).

The measurements were conducted at the D17 reflectometer[36] operated in time of flight mode at the ILL, Grenoble (France) with a wavelength range from 2 to 20 Å, giving a *q*-range

Table 2 Composition and contrasts of modified DPPC bilayers for neutron reflectivity experiments

Sample	1st layer	2nd layer
1 : 9	Pure DPPC-d_{62}	10 mol% SAP-6k–DPPC-d_{62}
2 : 8	Pure DPPC-d_{62}	20 mol% SAP-6k–DPPC-d_{62}

for specular reflectivity of 0.005–0.3 $Å^{-1}$. Each measurement is performed at two reflection angles, $\Theta_1 = 0.8°$ (resolution $\Delta q/q$ = 2.7%) and $\Theta_2 = 3.2$ (resolution $\Delta q/q$ varied linearly from 3.8% to 13%).[36] The detector efficiency was calibrated with H_2O. For the actual experiment the neutron beam enters the silicon substrate through one 5 × 1 cm^2 side of the block, hits at grazing incidence the polished 5 × 5 cm^2 face on which the layer under study has been deposited, and goes out through the opposite 5 × 1 cm^2 side.[31] Two direct beams have been measured at the settings of the two angles of incidence for data normalization. Each sample has been measured at three different solvent contrasts, such as H_2O (SLD = -0.56×10^{-6} $Å^{-2}$), 4 matched water (4MW, SLD = 4.0×10^{-6} $Å^{-2}$) and D_2O (SLD = 6.34×10^{-6} $Å^{-2}$).

Furthermore, for both samples, measurements at two different temperatures (25 °C and 50 °C) were carried out. The temperature is monitored using a thermocouple (equilibration time 25 minutes, stability <0.1 °C, absolute precision <0.3 °C), in the water-regulated sample chamber described in ref. 31. For annealing, one heating and cooling cycle was performed prior to the actual measurement.

3 Results

3.1 Langmuir isotherms

Fig. 2A shows the Langmuir isotherms for the cholesteryl α-CD anchor without polymer and the different SAPs listed in Table 1. The cholesteryl α-CD anchor themselves as well as the SAPs form stable monolayers at the air–water interface. Isotherms can be recorded until film collapse for surface pressures beyond 50 mN m^{-1}. This is in contrast to Langmuir isotherms attempted for end-capped PEG without CD anchors, which collapse around 12 mN m^{-1} due to the loss of PEG molecules into the subphase (isotherms not shown).[37]

The isotherms for all investigated SAPs are qualitatively similar with a plateau region for intermediate surface pressures (~10 mN m^{-1}) and very large molecular areas. The onset of the surface pressure rise, as well as the molecular area range over which the plateau extends, increases with increasing polymer MW (Fig. 2A). The shift to larger surface areas simply reflects the increased number of monomers N with MW.

At high surface pressures isotherms for pure SAP scale with the average number of threaded CDs which is illustrated in the inset of Fig. 2A, where the isotherms are plotted with the surface area normalized with respect to the number of CDs per SAP, A/N_{CD}. They all coincide fairly well for Π > 30 mN m^{-1}, yet are displaced to smaller areas compared to the isotherm of the pure α-CD anchor, probably caused by the loss of material into the subphase throughout compression.

Fig. 2B displays the compression isotherms for SAP-6k–DPPC mixed monolayers at different molar ratios. The isotherms for mixed monolayers with the other SAPs listed in Table 1 can be found in the ESI.† The plateau, indicating the DPPC liquid – condensed phase transition (Π = 5–6 mN m^{-1} for pure DPPC at 20 °C[23]), is not visible anymore when SAPs are present. The isotherms for the SAP–DPPC mixtures show the same features as the pure SAPs. The plateau region at 10 mN

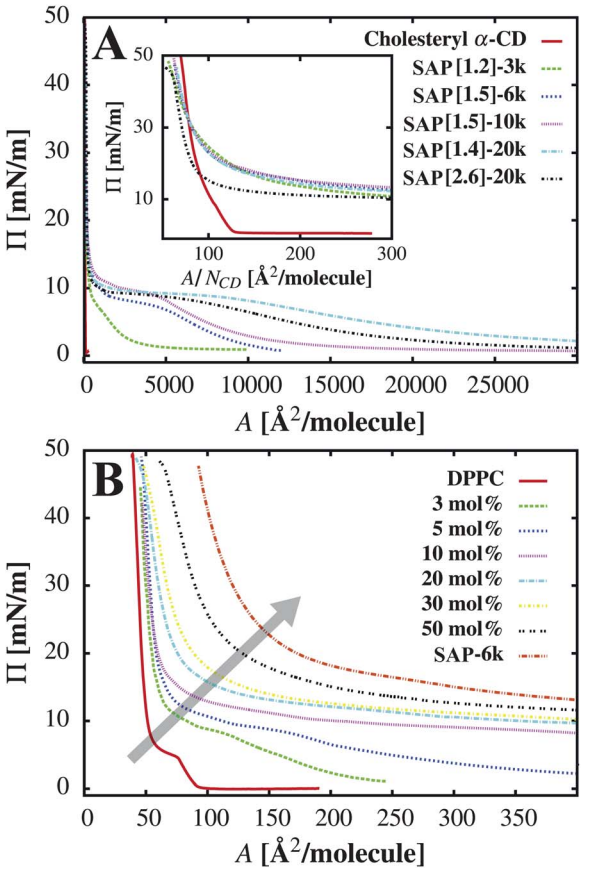

Fig. 2 (A) Langmuir isotherms at 20 °C for several SAPs compared to the cholesteryl α-CD anchor without polymer. The inset shows a zoom in surface area region between 0 and 300 $Å^2$ per molecule with the surface area normalised with respect to the number of CDs A/N_{CD}. (B) Langmuir isotherms for SAP-6–DPPC mixtures at 20 °C. The arrow indicates increasing molar ratios SAP.

m^{-1} is shifted to higher surface areas and surface pressures with increasing SAP content (indicated by an arrow in Fig. 2), reflecting the increased polymer density ($\sigma = 1/A$) in the monolayer. At high surface pressures they are slightly shifted to larger surface areas with respect to DPPC. For SAP molar ratios >30 mol% the shift is more pronounced.

3.2 Infra-red reflection-absorption spectroscopy (IRRAS)

We have measured IRRAS spectra for pure DPPC and cholesteryl α-CD monolayers simultaneously to recording compression isotherms. They have served as a reference for the analysis of the data acquired during compression of pure SAP-6k and SAP-6k–DPPC mixed monolayers.

Fig. 3 shows the representative spectra obtained for the SAP–DPPC mixture. Broad signals appear in the regions between 3000–2800 cm^{-1} and in the region between 1200–1000 cm^{-1} for surface pressures >10 mN m^{-1} when SAP is present in the monolayer. This is in contrast to pure DPPC and cholesteryl α-CD films, where peaks have already been observed for surface pressures >1 mN m^{-1}. At 5 mN m^{-1}, a considerable amount of PEG is adsorbed flatly on the surface and the DPPC molecules at

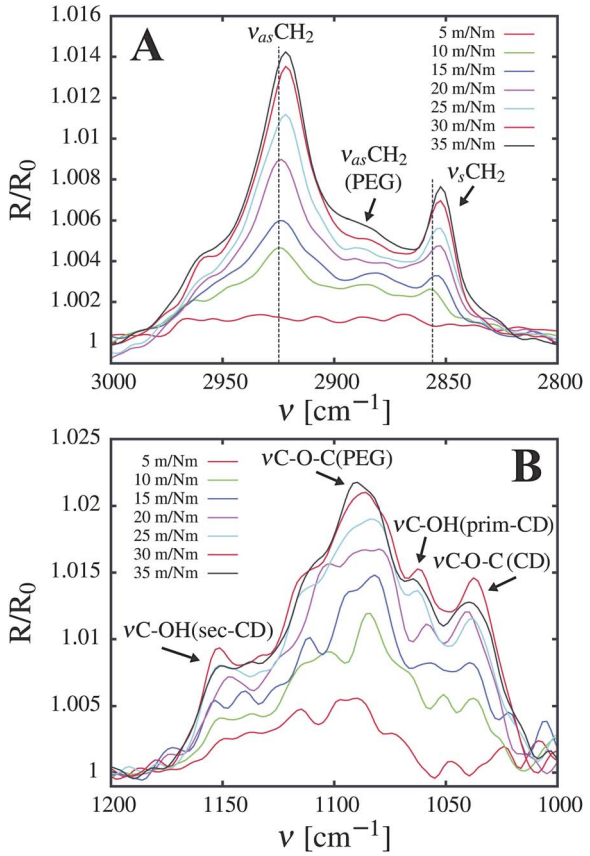

Fig. 3 Overlaid IRRAS spectra of (A) the CH_2 stretching region and (B) the C–O stretching region obtained during the compression of a 30 mol% SAP-6k–DPPC mixed monolayer. The surface pressures are measured at an interval of 5 mN m^{-1} from 5 to 35 mN m^{-1}, from the least to most intense bands, respectively.

this pressure have a lower surface density than the corresponding pure DPPC monolayer. Thus we do not detect any DPPC signal, but see instead a weak PEG contribution. The DPPC and SAP peaks became significant only above 10 mN m^{-1} when the free PEG is completely desorbed from the surface. In all cases the signal intensity increases with compression.

According to the literature, the large peak between 3000–2800 cm^{-1} displayed in Fig. 3A arises from the methylene stretching vibrations.[38] The individual peaks can be clearly assigned by comparison of the spectra of the pure compounds and deconvolution of the broad signal by a fitting with a Voigt type band shape model. The peak is composed of the symmetric and asymmetric CH_2 stretching modes at $\nu_sCH_2 \sim 2850$ and $\nu_{as}CH_2 \sim 2920$ cm^{-1}, respectively, along with the asymmetric methyl stretch at $\nu_{as}CH_3 \sim 2960$ cm^{-1} typical for DPPC.[39] Furthermore we find an asymmetric stretching vibration arising from the PEG $\nu_{as}CH_2 \sim 2885$.[40] As highlighted in Fig. 3A both the symmetric and asymmetric methylene peak frequencies, which are sensitive to the molecular order of the alkyl chains of DPPC,[41] decrease with increasing surface pressure. As shown in Fig. 4 the frequency shift occurs at higher surface pressures for the SAP–DPPC mixture compared to pure DPPC. Additionally the frequencies are shifted to higher frequencies for the SAP–DPPC mixed monolayer.

Fig. 3B shows the broad signal in the range of 1200–1000 cm^{-1}, which can be mainly attributed to the C–O stretching vibrations.[42] By comparison with the spectra of pure cholesteryl α-CD and SAP, as well as by deconvolution of the signal, the C–O stretching band of the SAP can be decomposed into signals arising from the threaded CD[43] and the strong ether C–O–C vibration modes typical for the PEG[42] (Fig. 3B). Thus it is possible to identify the primary and secondary C–OH vibrations (1061 ± 1 cm^{-1} and 1153 ± 1 cm^{-1}), as well as the acetal vibrations of the threaded CD ring (1036 ± 1 cm^{-1}). The peaks between 1080–1140 cm^{-1} can be related to the ether C–O vibration of the PEG. The complexity of the broad C–O absorption peak allows only for the identification of three subpeaks of the C–O ether vibration (instead of four described in the literature[40,44]), and only the asymmetric vibration ν_{as}C–O ∼ 1081 ± 1 cm^{-1} can be unambiguously assigned. Since the peaks in the C–O region do not shift systematically with compression, the given frequency values are averaged over different surface pressures.

3.3 Neutron reflectivity of monolayers containing SAPs

Fitting model. The film structure perpendicular to the air–water interface has been studied for monolayers containing SAP-6k or binary mixtures with DPPC using neutron reflectivity. The monolayer data were fitted using a three-layer model with three distinct regions of scattering length densities and corresponding thicknesses (Fig. 5). The first two layers represent the hydrophobic tails (DPPC alkyl chains and cholesterol part of SAP) and hydrophobic headgroups (DPPC phosphocholine head and CD moiety of SAP). Additionally a third layer representing the PEG chains has to be added. In agreement with the literature,[45] the data for SAPs cannot be well fitted using a simple steplike profile for the polymer layer (constant polymer concentration, ϕ_0 in the brush). As SAP polymer brushes should behave like normal chains grafted with one end to the surface,[16]

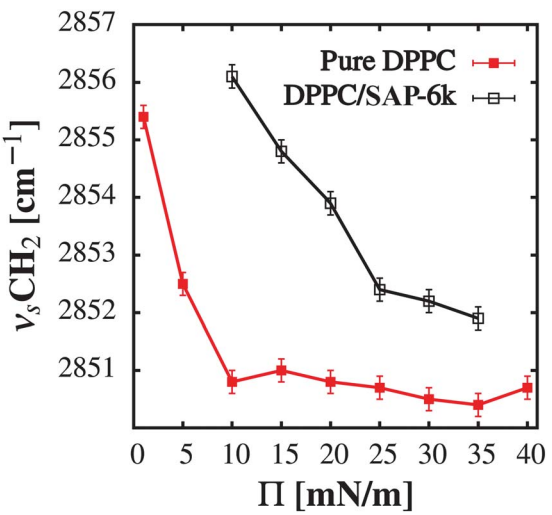

Fig. 4 Comparison of the frequency shift of symmetric ν_sCH_2 stretching vibrations between pure DPPC and a DPPC/STl mixture depending on the surface pressures. The frequencies have been determined from fits of the methylene region between 3000–2800 cm^{-1}. The error bars are in the order of ±0.2 cm^{-1}.

we used the standard parabolic density profile, which has already been used to successfully describe systems containing polymer brushes:[45,46]

$$\phi(z) = \frac{\pi^2}{8\,N^2 v}\left[1 - \left(\frac{z}{H}\right)^2\right], \quad (1)$$

with the polymer volume fraction at the interface ϕ_0 expressed by

$$\phi_0 = \frac{\pi^2}{8N^2 v}. \quad (2)$$

Since we know N and the scattering length density of PEG ($SLD_{PEG} = 0.64 \times 10^{-6}$ Å^{-2}), the polymer layer is determined by two independent fitted parameters, the brush thickness H and the polymer fraction at the headgroup–PEG interface ϕ_0. To reduce the number of fitting variables, we constrained the roughness of all layers to be the same.

For low polymer surface densities (3 mol% SAP–DPPC monolayer), we additionally have tested fitting the data with a polymer profile for sliding mushrooms, derived from a theoretical expression described by Baulin *et al.*:[16]

$$c(z,N) = \frac{2N}{\sqrt{\pi}R_g}\left[2\exp\left(-\frac{z^2}{4{R_g}^2}\right) - \frac{3\sqrt{\pi}}{R_g}\mathrm{erfc}\left(\frac{z}{2R_g}\right)\right] - \frac{2N}{\sqrt{\pi}R_g}\left[2\exp\left(-\frac{z^2}{{R_g}^2}\right) - \frac{2z\sqrt{\pi}}{R_g}\mathrm{erfc}\left(\frac{z}{R_g}\right)\right], \quad (3)$$

whereas R_g is substituted by $R_g = \sqrt{Na^2/6}$ with the monomer size a (3.5 Å for PEG[47]) and where erfc(x) is the complementary error function.[48] In this case the polymer layer is defined by the single adjustable parameter ϕ_0.

We use the parameters obtained for the DPPC monolayer as a reference for fitting the mixed films. The results for the head and tail layers are used as starting values, which are then refined. The roughness is constrained to be the same for heads and tails. To account for capillary waves at the air–water interface, the subphase roughness is fixed to 3 Å.

The water content x of the headgroup layer is calculated using the scattering length density of the subphase SLD_{sub}, the measured scattering length density for the headgroup layer SLD_x and the theoretical scattering length density for the headgroup layer SLD_t. The latter was estimated from the ratio of DPPC–SAP in the monolayer using the SLD values for phosphocholine and the CD residue of the SAP which are listed in the ESI:†

$$x = \frac{SLD_x - SLD_t}{SLD_{sub} - SLD_t}. \quad (4)$$

The results obtained from the fits for monolayers containing SAP-6k are listed in Table 3.

Pure monolayers SAP-6k. For surface pressures below the SAPs desorption transition (curve recorded at 9 mN m^{-1}), one box with a thickness of ~10 Å and the SLD expected for a combination of highly hydrated PEG and the cholesteryl CD anchor is sufficient to fit the data. This shows that the PEG chains are adsorbed to the interface together with the CD anchor.

For surface pressures above the desorption transition, the curves are very well fitted with the three layer model, consisting of a tail layer with very low SLD corresponding to the cholesteryl

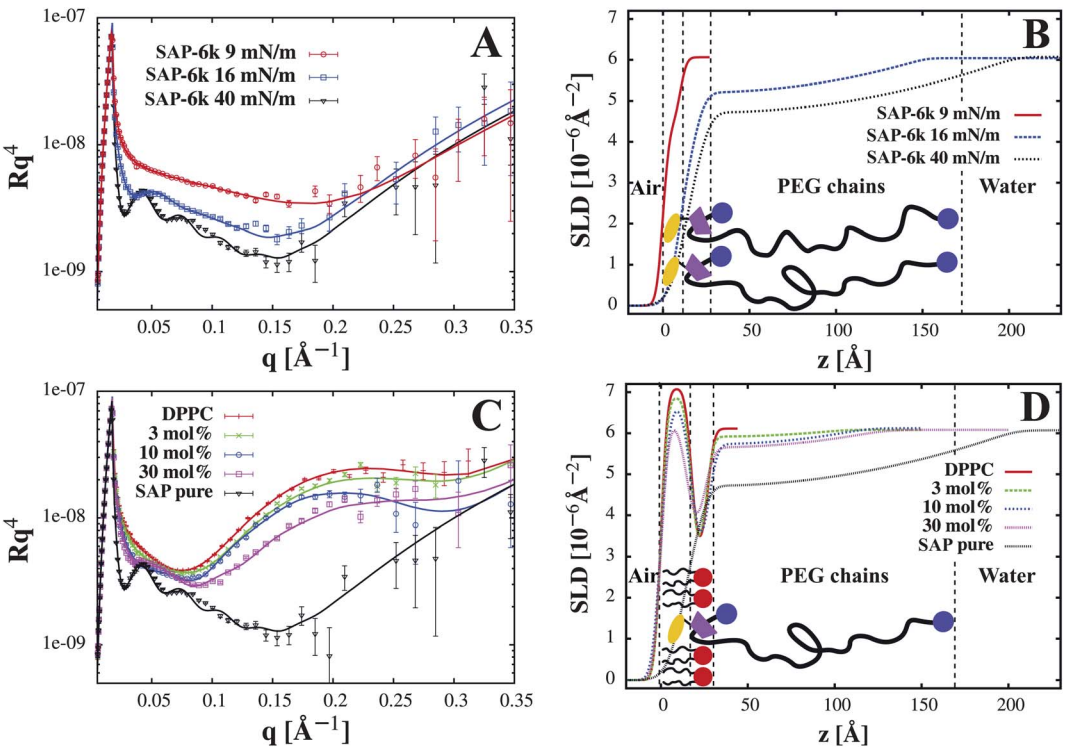

Fig. 5 Neutron reflectivity curves for pure SAP-6k monolayers at different Π (A) and corresponding SLD profiles (B), as well as for mixed SAP-6k–DPPC monolayers with different molar ratios SAP-6k at Π = 40 mN m^{-1} (C) and corresponding SLD profiles (D).

anchor, a hydrated headgroup layer which mainly consists of the CD with the complexed polymer in its cavity and a polymer part, best described with a parabolic density profile for polymer brushes (Fig. 5A and B). The cholesteryl slab thickness increases slightly with surface pressure. The head layer thickness remains constant. However its hydration decreases upon compression. Furthermore a very high roughness ~6.5 Å is found. Similar behavior has been observed for pegylated lipids.[45,46] The polymer volume fraction ϕ_0, as well as the brush thickness H, increases with compression, due to the increase in polymer density.

Mixed monolayers of SAP-6k–DPPC. Below the desorption transition, the data can be fitted well with a simple two box model without a polymer layer, similar to the DPPC–PEG mixtures without an anchor. The SLD profiles and the low thickness of the tail layer clearly indicate adsorbed SAP polymer chains together with DPPC at the interface (see results for 3 mol% SAP at 8 mN m^{-1} in Table 3).

Above the desorption transition (Π > 10 mN m^{-1}) all SAP–DPPC curves can be fitted very well with the parabolic profile for polymer brushes (Fig. 5C and D). The low polymer density 3 mol % SAP mixture could also be successfully fitted with the sliding mushroom polymer model (eqn (3)) using similar polymer volume fractions Φ as obtained with the parabolic model (Fig. 7). For higher molar fractions of SAP good fits were only obtained with the parabolic model.

Two well defined slabs correspond to the DPPC layer with the incorporated cholesteryl α-CD moiety of the SAP. The tail SLD is decreased according to the molar ratio of the incorporated SAP cholesteryl anchor with its low SLD. The head group layer is similar to the one found for pure DPPC since the thickness and SLD of the CD are not very different from the DPPC headgroup. The roughness is high compared to pure DPPC, yet smaller than for pure SAP.

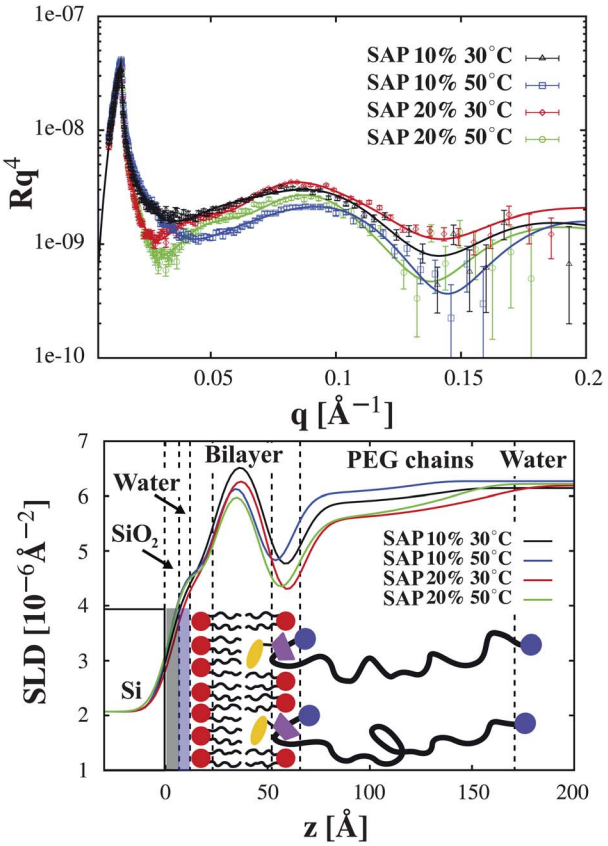

Fig. 6 Neutron reflectivity curves (top) and corresponding SLD profiles (bottom) for bilayers with a first layer of pure DPPC and a second mixed layer of SAP-6k–DPPC with different molar ratios of SAP-6k at 30 and 55 °C.

The brush height H and volume fraction ϕ_0 both increase with the polymer surface density, controlled by the SAP molar ratio, and with the compression of the monolayer (Fig. 5D). Only

Table 3 Fitting results for the SAP–DPPC-D_{62} monolayers at different surface pressures. l_x is the thickness, SLD_x the scattering length density of slab x, H the polymer layer thickness and ϕ_0 the volume fraction of the polymer at the head–polymer layer interface

Π [mN m^{-1}]	A_{iso} [Å^2]	A_n [Å]	ϕ_0	H [Å]	l_{head}	SLD_{head} [10^{-6} Å^{-2}]	Water [%]	l_{tail} [Å]	SLD_{tail} [10^{-6} Å^{-2}]	Roughness [Å]
Pure SAP-6k										
9	2000	—	—	—	—	—		10.1	4.3	3.0
16	200	560	0.16	134	10.4	3.41	28	9.6	0.12	6
40	120	270	0.26	178	10.6	3.10	20	11.6	0.16	6.5
SAP-6k 3 mol%										
8	5500		—	—	9.3	3.98		6.7	5.86	3.0
15	2333	8190	0.02	65	9.3	3.45	40	11.5	6.95	3.7
30	1667	5910	0.03	74	9.5	3.15	33	17.3	6.96	3.5
SAP-6k 10 mol%										
10	1200	6600	0.04	53	9.3	3.65	43	8.8	6.55	3.6
15	700	2520	0.06	81	9.4	3.41	38	11.2	6.63	3.5
40	500	1960	0.07	88	9.8	2.98	28	17.9	6.58	4
50	450	1570	0.08	99	9.7	2.92	27	18.7	6.64	4
SAP-6k 30 mol%										
16	233	690	0.14	130	10.4	3.6	40	9.9	6.38	3.8
40	167	1290	0.09	110	9.45	3.35	34	17.8	6.35	3.9
Errors	±10	±100	±0.01	±10	±0.5	±0.2	±5	±0.5	±0.2	±0.5

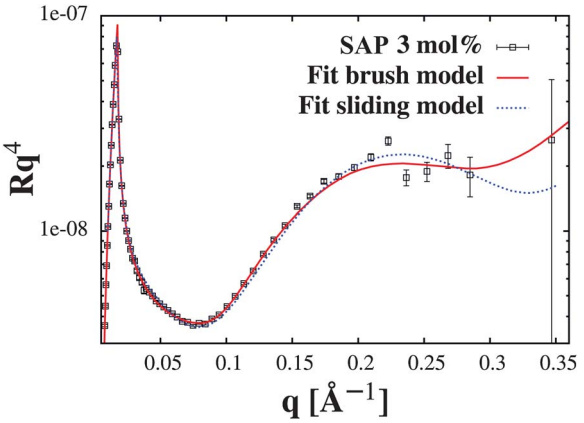

Fig. 7 Comparison between fits using the sliding model and the parabolic model for the SAP 3 mol% monolayer at 40 mN m^{-1}.

for the 30 mol% mixture is a smaller brush found for higher surface pressures, probably due to the loss of some of the SAPs into the subphase for high compressions. Also for surface pressures between 10 and 20 mN m^{-1}, above the desorption transition of the polymer and below the LE-LC phase transition of DPPC, polymer brushes are observed. This demonstrates that the SAP is also well anchored in LE phase DPPC and that the desorption of the polymer is independent from the phase state of DPPC.

3.4 Neutron reflectivity of bilayers containing SAPs

Fitting model. For the SAP/phospholipid bilayers, a 6 layer model has been adopted (see Fig. 6 (bottom)). It consists of a polymer layer already described for SAP monolayers, an outer headgroup slab with inserted CD moiety, a hydrophobic layer composed of phospholipid tails and the cholesteryl residues and a phospholipid headgroup layer close to the silicon substrate. Furthermore there is a thin water layer between the membrane and the substrate as well as a SiO_2 layer on the silicon block.

The fits for different contrasts have been performed in a coupled manner (see Fig. 6 (top)). Only the subphase scattering length density is changed for different contrasts. The results fall within the error bars if they still give satisfactory fits for all measured contrasts. Good coupled fits could be obtained for all measured samples at different temperatures in the q-range from 0.01 to 0.25 $Å^{-1}$. The detailed fitting results can be found in the ESI.†

Silicon substrates were characterized first, leading to a SiO_2 layer, 8 Å thick with a roughness ~6 Å. These parameters have been constrained to these values for fitting the supported bilayer experiments. A water layer of 4–6 Å thickness with a roughness between 5–7 Å has to be systematically added between the substrate and the membrane for all samples and temperatures. The found water layers are in agreement with comparable literature values.[31,32]

Supported bilayers modified with SAPs. For all measured SAP bilayers we identify two headgroup regions, one single central tail layer, as well as a polymer brush layer. To obtain good fits a roughness between 8–10 Å had to be added between the layers, which is larger by several Angstroms compared to supported DPPC membranes[31,49] and to supported bilayers modified with amphiphilic CDs.[23]

For the bilayers, which are composed of a first DPPC-d_{62} monolayer, and a 2nd mixed SAP-6k–DPPC-d_{62} monolayer, the data obtained for the headgroup layer close to the silicon substrate are consistent with values previously described in the literature.[31,32] The tail region decreases slightly in thickness with an increase in the SAP content (30.5 for 10 mol% SAP and 29.5 Å for 20 mol% SAP). Accordingly the SLD is decreased compared to pure DPPC chains according to the molar ratio of SAP due to the presence of the cholesteryl anchors with very low SLD. Furthermore a typical water content in the order of 10% had to be added to account for holes in the bilayer. The measured bilayers with different SAP contents are stable also when undergoing temperature cycles. Upon heating from 30 to 50 °C a thickness decrease ~5 Å has been observed, since the DPPC aliphatic chains undergo a gel–lipid gel transition in this temperature range.[50] This is also reflected in the total bilayer thickness without considering the polymer layer (49 to 44 Å for 10 mol% SAP and 51 to 47 Å for 20 mol% SAP). The outer mixed headgroup layer with the inserted CD moieties of the SAPs increases in thickness with SAP content and has been found to be considerably thicker compared to pure phosphocholine heads. Using classical values for SLDs (see ESI,† Table S1) and taking into account the SAP molar ratios, we find a water content which is somewhat smaller than for the pure headgroup layer.

The polymer layer is well described by the parabolic profile already used to describe the monolayers. As expected, it is highly hydrated with a height H and volume fraction of the polymer ϕ_0 both increasing with the polymer surface density controlled by the SAP molar ratio. Upon heating, H decreases ~10 Å. Furthermore the findings for the polymer brush in the bilayer are in very good agreement with the monolayer data for the corresponding SAP ratios.

4 Discussion

4.1 Amphiphilic properties of SAPs

The isotherms for pure SAPs and SAP–DPPC mixtures are in good agreement with isotherms for comparable modified PEGs described in the literature, such as styrene–PEG block copolymers[29] or pegylated lipids.[30,40] The presence of the characteristic peaks for the CD anchor and PEG up to high surface pressures proves that the cholesteryl α-CD moiety firmly anchors the SAPs at the air–water interface in analogy to the cholesteryl CDs studied recently.[51,52] In contrast, the endcapped polymers are expelled to the subphase, which proves that anchoring of the SAPs is truly governed by the cholesteryl CD anchor and not mediated by the hydrophobic DMPE stopper molecules.

The SAP isotherms exhibit three different regions upon compression, which correspond to different chain conformations and are typical of hydrophobically modified PEGs.[29,53] The

neutron reflectivity results clearly show that at low compression, the PEG chains adsorb at the air–water interface together with the cholesteryl CD membrane anchor due to the amphiphilic nature of the ethylene glycol (EG) monomers. The interaction between the EG monomers and the interface is attractive, and the EG adsorbs at the air–water interface with adsorption energies in the order of one k_BT per monomer.[29] In this regime the pressure and the shape of the isotherm are mainly determined by the number of monomers in the layer. Starting at the plateau region in the isotherm, the cholesteryl CD anchor gradually covers the whole interface and forms a well defined cholesteryl CD layer, as evidenced by neutron reflectivity and by the sharp CD signals in the IRRAS spectra. Thus the EG-interface interaction becomes repulsive due to repulsive interactions between EG residues and the cholesteryl CD anchor. This leads to the desorption of the EG monomers from the surface and the formation of a SAP polymer brush at the sharp rise of the isotherms, manifested in the appearance of the PEG signals in IRRAS. The presence of the characteristic peaks for the CD anchor and PEG up to high compressions is a qualitative proof that the SAPs are firmly anchored at the interface. The broad shape of the C–O band without sharp peaks is typical for an amorphous PEG structure[54] and corresponds very well to observations made for polymer brushes formed with lipopolymers.[40,42]

4.2 Insertion of SAPs into DPPC model membranes

Monolayers. Our results show that SAPs readily insert into DPPC model membranes due to their α-CD anchor, since stable isotherms can be recorded for any kind of molar ratio, similar to cholesteryl CDs described recently.[23,51] Our data are also in good agreement with comparable pegylated lipid–phospholipid mixtures.[30] IRRAS spectra exhibit the typical signals for the SAP and the DPPC up to high compressions which show that the SAPs remain well inserted into the phospholipid monolayer. The SAPs have a fluidising effect on the monolayer, shifting the LE–LC phase transition and decreasing the alkyl chain ordering. This effect is shown in Fig. 4, where the methylene shifts for pure DPPC and the SAP mixtures are compared. The characteristic shift of the DPPC methylene peaks occurs at much higher surface pressures for the film containing SAP. Furthermore the shift is less pronounced, indicating that the SAPs perturb the alkyl chain ordering. As reported recently for cholesteryl CD–DPPC mixtures,[23] it is likely that not only the PEG chains but also the cholesteryl CD residues influence the DPPC phase transition. Yet it is difficult to distinguish the effect of the polymer tether and the effect of the cholesteryl anchor on the alkyl chain ordering.

With the help of neutron reflectivity we have obtained an insight into the film structure upon compression. Similar to pure SAP monolayers, below the desorption plateau the polymer is adsorbed to the interface. Above the desorption transition, a well-defined DPPC layer with the incorporated cholesteryl α-CD anchor of the SAP is formed at the interface. Moreover the PEG chains form polymer brushes, which increase in thickness with SAP surface density.

Phase behavior. Monolayer in-plane morphology has been investigated by means of Langmuir isotherms, Brewster Angle Microscopy (BAM) and Atomic Force Microscopy (AFM). BAM and AFM images are reported in the ESI.† Considering the images for SAP and PEG-cap–DPPC mixtures, our findings can be summarized as follows: at surface pressures below the desorption transition plateau, SAP and PEG–DPPC mixtures behave similarly. For both, a phase separation is observed between the phospholipids and the polymer chains adsorbed to the surface. Although the typical plateau for the LE–LC of DPPC is not visible in the isotherms, the phase change is clearly visible in the images. Increasing molar ratios of SAP influence the alkyl chain condensation because the appearance of the DPPC LC phase is shifted to higher surface pressures.

In SAP mixtures, the LC phase domains are evenly distributed on a uniform surface, consisting of mixed LE DPPC and SAP. Upon further compression the LC domains grow and become denser until a contrast inversion is observed in a honeycomb-like pattern. At high surface pressures we find a phase separated mixed monolayer of DPPC in the LC state and the SAP cholesteryl-CD anchor with its PEG tether submerged in the subphase. The film morphology at high surface pressures as well as the comparison with layers of PEG without a CD anchor demonstrate that the SAPs are firmly anchored into the DPPC monolayers.

Bilayers. Stable bilayers modified with SAPs can be readily prepared. The values obtained for the polymer brush are in very good agreement with the corresponding monolayer data. The schematic structure is illustrated in Fig. 6. The bilayers undergo a gel–liquid phase transition upon heating, whereas the SAPs remain well inserted. However at high temperature the brush height is diminished, which can be explained by changes in solvent conditions at higher temperatures. The roughness has higher values than those of CD modified bilayers described in the literature,[23] which shows that the polymer perturbs the bilayer.

Available surface area per polymer. To investigate the possible dissolution of SAP molecules in the subphase, the available polymer surface area A_{iso}, estimated from the isotherms, is compared to the area per chain A_n calculated from the neutron data. A_{iso} is obtained using the surface area A from the isotherm and the molar fraction of SAP, x_{SAP}:

$$A_{iso} = A/x_{SAP} \tag{5}$$

A_n is calculated from the reflectivity data by integrating the volume fraction profile $\phi(z)$:

$$A_n = \frac{N v_{EG}}{\int_0^H \phi(z)\mathrm{d}z}, \quad \text{with } \phi(z) = \phi_0\left[1 - \left(\frac{z}{H}\right)^2\right] \tag{6}$$

where N is the chain length and $v_{EG} = 61.4$ Å^3 is the volume of an EG monomer.[45]

Values for A_{iso} and A_n are reported in Table 3. A large difference is systematically observed, A_n being 2–4 times larger than A_{iso}. A_n is the more reliable value since it reflects the actual amount of substance at the interface.[45] This discrepancy can be

attributed to the loss of material into the subphase during compression. The large difference between A_n and A_{iso} is an indication that in addition to the loss of the PEG fraction without a cholesteryl CD anchor, also some of the SAP is expelled from the interface. This is *e.g.* manifested in the decreased brush thickness for high surface pressure found for the 30 mol% SAP monolayer.

4.3 Sliding effect

The additional conformational freedom in sliding grafted polymer layers should induce important differences in the equilibrium and dynamic behavior compared to polymer tethers grafted on a fixed point. According to the theory by Baulin *et al.*,[16] the polymer conformation should depend on the grafting density. For sliding mushrooms (assuming Gaussian chains), they found that the low density grafts mainly adopt symmetric configurations with an equal number of chains at each side of the sliding ring. This translates into a decreased polymer layer thickness compared to conventional polymer grafts with the same N. However densely grafted polymer brushes adopt stretched asymmetric configurations.[16] Therefore they should essentially behave like normal polymer brushes grafted with a fixed link.

Sliding mushrooms. The sliding ability of the SAPs should have the greatest impact on the polymer conformation in the mushroom regime. Thus for SAPs in the mushroom regime, eqn (3) can be tested to describe the polymer layer in the fit model for the neutron experiments instead of the parabolic profile. For SAP-6k we should find the PEG tethers in the mushroom regime, when the available surface area per polymer fulfills the criterion $A \geq R_F^2$ ($R_F^2 \approx 5000$ Å^2). As expected, attempting to fit data with SAP ratios larger than 3 mol% ($A < R_F^2$) with the sliding model results in very bad fits. Fitting the data for the mixed SAP–DPPC monolayer with 3 mol% SAP, where $A \geq R_F^2$ holds, gives almost as good results as with the sliding model (Fig. 7), the polymer concentration profile can thus be equally well described by both the sliding and the brush model.

This suggests that for 3 mol% SAP the PEG chains are in an intermediate regime between the non-interacting sliding mushrooms and the brush configuration. Hence smaller SAP ratios would need to be tested with polymer densities low enough to unambiguously find the tethers in the mushroom regime. However we find that already for the 3 mol% SAP film, the impact of the polymer tether on the scattering curves is small, close to the detection limit.

Sliding brushes. For the brush regime the theory of sliding grafted polymer layers predicts that they should behave like normal brushes. In this case, according to mean field theory,[2] the brush height H scales linearly with $(\phi_0)^{1/2}$. The relationship also holds if material is lost into the subphase since H and ϕ_0 depend only on the actual polymer density. Fig. 8 displays the scaling between brush height H and $(\phi_0)^{1/2}$ for the monolayer data, measured above the desorption transition (blue crosses) and the bilayers (red dots), successfully fitted with the parabolic profile.

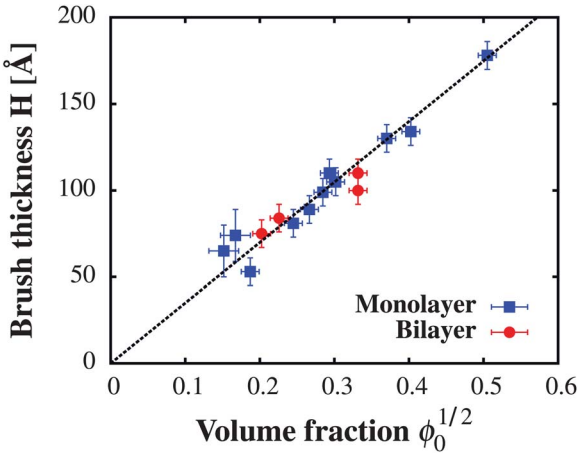

Fig. 8 Scaling of the brush height H with $(\phi_0)^{1/2}$. The dashed line represents the best linear fit. The plotted data can be found in Table 3.

Within the error bars, all points fall on the scaling line predicted by the mean field theory, showing that in the brush regime the sliding ligands indeed behave as end grafted polymers.

5 Conclusions

A detailed understanding of the interfacial properties of SAPs as well as the insertion properties into phospholipid membranes has been obtained. At first we have shown that the cholesteryl α-CD is suitable for anchoring the SAPs at the air–water interface and for insertion into phospholipid monolayers and bilayers. For sufficiently high polymer surface densities they form polymer brushes, which follow the scaling laws predicted by polymer theory. The dense SAP layers display the conventional behavior of end-grafted polymer brushes, in agreement with the theoretical description for grafts of sliding polymers, where asymmetric chain conformations are predicted for high surface densities. In the mushroom regime, theory foresees symmetric chain conformations which lead to reduced polymer layer thickness compared to layers fixed at one chain end. The distinct behavior of sliding grafts has not been fully investigated so far due to experimental constraints of the methods used for the SAP characterisation.

Although the SAPs are firmly anchored at the interface, loss of material into the subphase occurs, as shown by comparison of the polymer surface areas in the isotherms with the ones computed from neutron data. Such a loss can be partly ascribed to the solution composition heterogeneities, a fraction of polymers without a cholesteryl CD-anchor is present in each of the investigated samples, but further loss of SAPs might also occur during compression.

It is expected that the ability of the SAP polymers to slide through the CD ring, and the associated modified distribution of chain ends, will translate into a new type of tethered ligand–receptor pairs. The study of such interactions, driven by sliding tethered ligands, could be performed *e.g.* by force measurements between two phospholipid bilayers, the first containing SAPs modified with a ligand end-group and the second, opposite bilayer, anchoring a complementary receptor moiety.

Acknowledgements

This work is supported by the French Research Program Slid-TetherLig ANR - 07 - NANO - 016 -02 and Region Alsace (Ph.D. Grant). The authors wish to thank the ILL for the award of beam-time and use of the PSCM facilities.

References

1 G. J. Fleer, M. A. Cohen Stuart, J. M. H. M. Scheutjens, T. Cosgrove and B. Vincent, *Polymers at Interfaces*, Chapman and Hall, London, 1993.
2 S. T. Milner, T. A. Witten and M. E. Cates, *Macromolecules*, 1988, **21**, 2610–2619.
3 R. Tuinier, J. Rieger and C. de Kruif, *Adv. Colloid Interface Sci.*, 2003, **103**, 1–31.
4 R. Yerushalmi-Rozen, J. Klein and L. J. Fetters, *Science*, 1994, **263**, 793–795.
5 D. D. Lasic and F. J. Martin, *Stealth Liposomes*, CRC Press, 1995.
6 P. Auroy, L. Auvray and L. Léger, *Phys. Rev. Lett.*, 1991, **66**, 719–722.
7 T. Bickel, C. Jeppesen and C. M. Marques, *Eur. Phys. J. E*, 2001, **4**, 33–43.
8 J. Klein, D. Perahia and S. Warburg, *Nature*, 1991, **352**, 143–145.
9 E. B. Zhulina, O. V. Borisov and T. M. Birshtein, *J. Phys. II France*, 1992, **2**, 63–74.
10 E. Evans and K. Ritchie, *Biophys. J.*, 1999, **76**, 2439–2447.
11 J. Pyun, T. Kowalewski and K. Matyjaszewski, *Macromol. Rapid Commun.*, 2003, **24**, 1043–1059.
12 P. Mansky, Y. Liu, E. Huang, T. P. Russell and C. Hawker, *Science*, 1997, **275**, 1458–1460.
13 O. Prucker and J. Rühe, *Macromolecules*, 1998, **31**, 592–601.
14 J. Rühe, *Macromol. Symp.*, 1998, **126**, 215–222.
15 A. Kenworthy, K. Hristova, D. Needham and T. McIntosh, *Biophys. J.*, 1995, **68**, 1921–1936.
16 V. A. Baulin, A. Johner and C. M. Marques, *Macromolecules*, 2005, **38**, 1434–1441.
17 A. Harada and M. Kamachi, *Macromolecules*, 1990, **23**, 2821–2823.
18 N. Yui, R. Katoono and A. Yamashita, *Inclusion Polymers*, Springer Berlin/Heidelberg, 2009, vol. 222, pp. 115–173.
19 K. Ito, *Polym. J.*, 2012, **44**, 38–41.
20 G. Fleury, G. Schlatter, C. Brochon, C. Travelet, A. Lapp, P. Lindner and G. Hadziioannou, *Macromolecules*, 2007, **40**, 535–543.
21 R. Auzely-Velty, B. Perly, O. Taché and T. Zemb, *Carbohydr. Res.*, 1999, **318**, 82–90.
22 M. Roux, B. Perly and F. Djedaini-Pilard, *Eur. Biophys. J.*, 2007, **36**, 861–867.
23 M. Bauer, T. Charitat, C. Fajolles, G. Fragneto and J. Daillant, *Soft Matter*, 2012, **8**, 942–953.
24 S. Beugin, K. Edwards, G. Karlsson, M. Ollivon and S. Lesieur, *Biophys. J.*, 1998, **74**, 3198–3210.
25 C. Carrion, J. Domingo and M. de Madariaga, *Chem. Phys. Lipids*, 2001, **113**, 97–110.
26 H. Xu, K. Q. Wang, Y. H. Deng and D. W. Chen, *Biomaterials*, 2010, **31**, 4757–4763.
27 G. Fleury, C. Brochon, G. Schlatter, G. Bonnet, A. Lapp and G. Hadziioannou, *Soft Matter*, 2005, **1**, 378–385.
28 V. Hong, S. I. Presolski, C. Ma and M. G. Finn, *Angew. Chem., Int. Ed.*, 2009, **48**, 9879–9883.
29 M. C. Fauré, P. Bassereau, L. T. Lee, A. Menelle and C. Lheveder, *Macromolecules*, 1999, **32**, 8538–8550.
30 M. M. Lozano and M. L. Longo, *Soft Matter*, 2009, **5**, 1822–1834.
31 T. Charitat, E. Bellet-Amalric, G. Fragneto and F. Graner, *Eur. Phys. J. B*, 1999, **8**, 583–593.
32 B. Koenig, S. Kureger, W. Orts, F. Majkrzak, N. Berk, J. Silverton and K. Gawritsch, *Langmuir*, 1996, **12**, 1343–1350.
33 O. Heavens, *Optical Properites of Thin Films*, Butterworth, 1955.
34 FIGARO, http://www.ill.eu/instruments-support/instruments-groups/instruments/figaro/.
35 R. Campbell, H. Wacklin, I. Sutton, R. Cubitt and G. Fragneto, *Eur. Phys. J. Plus*, 2011, **126**, 1–22.
36 R. Cubitt and G. Fragneto, *Appl. Phys. A: Mater. Sci. Process*, 2002, **74**, 329–331.
37 M. Winterhalter, H. Bürner, S. Marzinka, R. Benz and J. Kasianowicz, *Biophys. J.*, 1995, **69**, 1372–1381.
38 R. Mendelsohn, G. R. Mao and C. R. Flach, *Biochim. Biophys. Acta, Biomembr.*, 2010, **1798**, 788–800.
39 C. R. Flach, F. G. Prendergast and R. Mendelsohn, *Biophys. J.*, 1996, **70**, 539–546.
40 T. Wiesenthal, T. R. Baekmark and R. Merkel, *Langmuir*, 1999, **15**, 6837–6844.
41 C. R. Flach, A. Gericke, J. W. Brauner and R. Mendelsohn, *Biophys. J.*, 1997, **72**, WP340.
42 T. R. Baekmark, T. Wiesenthal, P. Kuhn, A. Albersdrfer, O. Nuyken and R. Merkel, *Langmuir*, 1999, **15**, 3616–3626.
43 R. Vico, R. de Rossi and B. Maggio, *Langmuir*, 2010, **11**, 8407–8413.
44 E. P. Enriquez and S. Granick, *Colloids Surf., A*, 1996, **113**, 11–17.
45 H. Bianco-Peled, Y. Dori, J. Schneider, L.-P. Sung, S. Satija and M. Tirrell, *Langmuir*, 2001, **17**, 6931–6937.
46 J. Majewski, T. L. Kuhl, M. C. Gerstenberg, J. N. Israelachvili and G. S. Smith, *J. Phys. Chem. B*, 1997, **101**, 3122–3129.
47 N. W. Moore and T. L. Kuhl, *Langmuir*, 2006, **22**, 8485–8491.
48 M. Abramovitz and I. Stegun, *Handbook of Mathematical Functions*, Dover, New York, 1965.
49 L. Malaquin, T. Charitat and J. Daillant, *Eur. Phys. J. E: Soft Matter Biol. Phys.*, 2010, **31**, 285–301.
50 Z. Leonenko, E. Finot, T. Dahms and D. Cramb, *Biophys. J.*, 2004, **86**, 3783–3793.
51 A. Klaus, C. Fajolles, M. Bauer, M. Collot, J.-M. Mallet and J. Daillant, *Langmuir*, 2011, **27**, 7580–7586.
52 M. Bauer, C. Fajolles, T. Charitat, H. Wacklin and J. Daillant, *J. Phys. Chem. B*, 2011, **115**, 15263–15270.
53 C. Barentin, P. Muller and J. F. Joanny, *Macromolecules*, 1998, **31**, 2198–2211.
54 M. Dissanayake and R. Frech, *Macromolecules*, 1995, **28**, 5312–5319.

